International Journal of Engineering & Technology, 7 (4.35) (2018) 796-802

International Journal of Engineering & Technology

Website: www.sciencepubco.com/index.php/IJET

Research paper

Numerical Investigation on Surface Coverage of Weakly-Adsorbed Molecular SO_2 Contaminant in a PEM Fuel Cell Cathode

Saiful Hasmady[1]*, Kazuyoshi Fushinobu[2]

[1]*Department of Mechanical Engineering, Universiti Tenaga Nasional, Malaysia*
[2]*Department of Mechanical & Control Engineering, Tokyo Institute of Technology, Japan*
**Corresponding author E-mail: saifady@uniten.edu.my*

Abstract

This paper describes attempt to numerically predict surface coverage of SO_2 contaminant in a PEMFC cathode, as a step towards assessing its impact towards cell performance. Three-dimensional macro-homogeneous conservation equations of two-phase fluid flow is coupled with micro-scale cathode ORR kinetics to solve for surface coverage distribution of O-ad and SO_2-ad at the surface of the catalyst layer for bulk SO_2 concentrations of 2.5 and 5.0 ppm. At 2.5 ppm, SO_2-ad is predicted to block ca. 20% of the active sites at cell current density of 0.2 A/cm^2. The effect of SO_2-ad blockage is then correlated with loss in cell performance. The numerical results are compared with experimental data from literature, which confirms that though the model successfully predicted higher potential loss with higher bulk SO_2 concentration in the reactant feed, inclusion of only weakly-adsorbed SO_2 will under-predict the exact potential loss experienced by the cell. This means strongly adsorbed sulfur containing species must be adopted into the model in order to better predict the severity of degradation of the cell due to SO_2 contamination.

Keywords: *PEM fuel cell, sulfur dioxide, contamination, surface coverage*

1. Introduction

Proton exchange membrane fuel cell (PEMFC) is a promising energy converter that can be installed as a power source in vehicles, be it land, sea or air. The cell's cathode electrode in practice obtain its oxygen supply by drawing in environmental air, which is susceptible to sulfur dioxide (SO_2) contamination should severe air pollution (for example, operating a rescue vehicle near a volcano) is encountered. With respect to SO_2, studies in [1 – 3] show that traces of SO_2 even in ppms, when in contact and reacted within the cathode electrocatalyst will cause degradation of performance and ultimately lower its long-term durability. This performance loss is believed mainly due to the unwanted adsorbate on the heterogeneous electrode catalyst decreasing available active platinum catalyst sites needed for the cathode oxygen reduction reaction (ORR) resulting to severe kinetic loss and performance deterioration. Mohtadi et al. [1] found that, based on accumulated total dosage of 118.5 µmol of SO_2 in air, PEMFC performance degraded by 53% at 2.5 ppm, and a higher 78% at 5 ppm with the same dosage. Their study illustrates higher PEMFC performance loss with SO_2 bulk concentration and dosage. This dependency warrants further investigation on identifying the underlying phenomena and the degradation mechanism. Since the mechanism of ORR itself is complex, the actual degradation pathway is still a subject of interest of many researchers. Baturina et al. [2] studied the effect of 1 ppm SO_2 in air on the performance of PEMFC cathode, and quantified the coverage of adsorbed sulfur species at three different potentials. Their cyclic voltammetry results show peaks attributed to weakly and strongly adsorbed sulfur (S-ad) blocking the sites available for ORR, with a cumulative total of ca. 30% blockage at 0.5 – 0.8 V operation. At 1 ppm, a -30 mV potential shift is observed, but since the Tafel slopes are of similar magnitude, they deduced that the underlying ORR mechanism itself is unaffected depending on potential. The potential shift not affecting ORR at high potentials (low current densities) is attributed to adsorption of SO_2, and later at low potentials (high current density) SO_2 started to be reduced to S-ad. The formation of S-ad is thought to originate from the electrochemical pathway following reduction of SO_2 as proposed by Contractor and Lal [4] with SO-ad intermediate. The adsorption process preceding the electrochemical reduction or decomposition of SO_2 is not specifically mentioned. Zhai et al. [5] investigated the effect of galvanostatically operating a PEMFC under SO_2 contamination by applying a constant current density of 0.6 A/cm^2 for 120 hours, contrary to the potentiostatic approach in [2]. It is found out that SO_2 poisoning process consisted of reversible and irreversible parts. The former is attributed to SO_2 concentration, and the latter is potential dependent, illustrating the effect of weakly and strongly adsorbed sulfur containing ad-species. Recently Punyawudho and co-workers [6] conducted oxygen-assisted temperature-programmed desorption (TPD) investigation on SO_2 adsorption on Pt/C electrocatalyst. They identified that on the catalyst surface SO_2 can be found as a weakly-adsorbed ad-species SO_2-ad, and strongly adsorbed ad-species postulated as a product of further dissociation of SO_2-ad into SO-ad and S-ad. Though the electrochemical pathway is not discussed, their method contributed kinetic data on SO_2 adsorption, which is still lacking to date.

In this study, an attempt is made in order to predict the effect of variation of bulk SO_2 concentration in the air feed towards the overall performance of the cell. Not much effort is seen in theoret-

ical studies and experimental investigation on SO_2 transport process inside the electrode of PEMFC. Experimentally, Tsushima et al. [7] investigated various concentrations of SO_2 up to 500 ppm at open circuit voltage (OCV) to better understand the influence of SO_2 concentration on the nature of SO_2 transport and adsorption on the membrane electrode assembly (MEA). They found out that as the SO_2 concentration increased, the degradation rate of the cell voltage increased as well, initially dominated by SO_2 transport due to the availability of free adsorption sites. As time progresses, a large amount of sulfur-containing species accumulated around the catalyst surface, and the cell voltage reached equilibrium. The effect of relative humidity (RH) is also discussed, which shows higher anode electrode performance loss at low RH, while the cathode electrode is mainly unaffected. A more dominant effect for cathode electrode performance loss due to SO_2 contamination is its potential, where after a certain value is reached, reduces SO_2-ad into S-ad, as mentioned before. Their previous work in [8] explained anode contamination of SO_2 to be originated from water containing dissolved SO_2 that is transported via diffusion across the membrane. On theoretical works, St-Pierre [9] developed a one-dimensional generic, transient mathematical model that predicts the kinetic loss for contaminants that partially cover the surface of PEMFC catalysts leaving irreversible products. Though generic, the work however is limited by the unavailability of many kinetic data, which impedes validation work. Further, the connection to transport phenomena is still missing. Shi and co-workers [10] also developed a similar model of one-dimensional generic capability. While developed mainly for toluene contamination, the model is not discussed in light with SO_2, and accordingly, limited by unavailability of kinetic data and the much-needed coupling with transport processes of the reactants.

This paper seeks to theoretically investigate the multicomponent transport of gas species containing molecular SO_2 inside a two-phase mixture setup, and explore its convection and diffusion phenomena towards the catalyst layer. Molecularly adsorbed SO_2 is modeled to block the active reaction sites on the Pt cathode electrocatalyst, and the apparent kinetics of the electrochemical reaction is coupled with two-phase macro-homogeneous conservation equations. This should serve as a precursor for the additional steps that may be present to interfere with the ORR.

2. System Schematic and Modeling Domain

The three-dimensional schematic of the cell and its domains is depicted in Fig. 1. The two-dimensional cross-sectional diagram showing the boundary conditions is shown in Fig. 2.

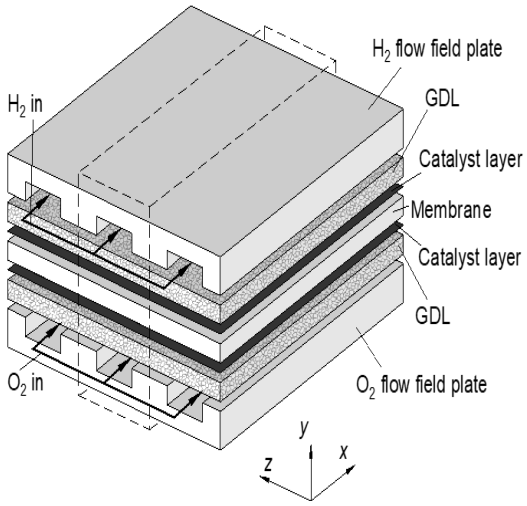

Fig. 1: Three-dimensional view of a single-cell PEMFC. Region enclosed by the dashed lines depicts a single channel with parallel-flow arrangement [11].

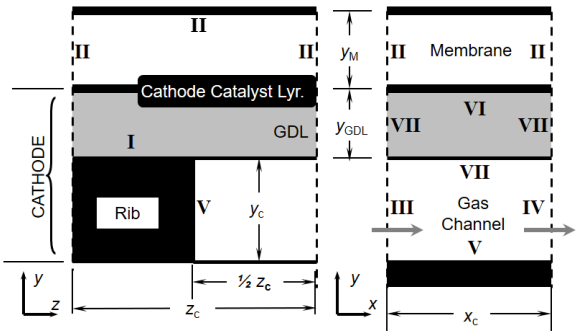

Fig. 2: Schematic of the 2D cross-section of the calculation domain detailing the boundary conditions.

3. Governing Equations

In this section, the macro-scale conservation equations of various transport variables in the PEMFC cathode are listed. The equations take the form of partial differential equations written in three-dimensions, and are essentially in two phases with multi-component species.

3.1. Macro-Homogeneous Transport Equations

In steady state and two phases, the governing equations for the processes that involve conservation of mass, momentum, chemical species, liquid water, electronic and ionic charge, as well as energy within the PEMFC cathode can be written in their three-dimensional forms as

Conservation of mass for a two-phase mixture:

$$\nabla\cdot(\varepsilon\rho\mathbf{u}) = 0 \tag{1}$$

Conservation of momentum for a two-phase mixture:

$$\nabla\cdot(\varepsilon\rho\mathbf{u}\mathbf{u}) = -\varepsilon\nabla P + \nabla\cdot(\varepsilon\mu\nabla\mathbf{u}) + S_{\text{mom}} \tag{2}$$

Conservation of multi-component chemical species in gaseous phase:

$$\nabla\cdot\left[\varepsilon(1-s)c\mathbf{u}_{\text{g}}X_i\right] = c\sum_{i=1}^{n-1}\nabla\cdot\left(D_{ij}^{\text{eff}}\nabla X_i\right) + S_{\text{spe},i} \text{ with } \sum_{i=1}^{n}X_i = 1 \tag{3}$$

Conservation of mass of water in liquid phase (liquid water saturation):

$$\nabla\cdot\left(\frac{\rho_{\text{l}}}{\rho_{\text{g}}}\frac{K_{\text{p}}}{\mu}\frac{\partial P_{\text{c}}}{\partial s}\nabla s + \varepsilon\rho\mathbf{u}\right)_{\text{l}} = S_{\text{liq}} \tag{4}$$

Conservation of electronic and ionic charge:

$$\nabla\cdot\left(\sigma_{\text{s}}^{\text{eff}}\nabla\phi_{\text{s}}\right) + S_{\text{ch,s}} = 0, \text{ and } \nabla\cdot\left(\sigma_{\text{p}}^{\text{eff}}\nabla\phi_{\text{M}}\right) + S_{\text{ch,M}} = 0 \tag{5}$$

Conservation of energy:

$$\nabla\cdot\left[\left(\rho c_{\text{p}}\right)^{\text{eff}}(\mathbf{u}T)\right] = \nabla\cdot\left(k^{\text{eff}}\nabla T\right) + S_{\text{ene}} \tag{6}$$

Membrane hydration:

$$-\frac{\rho_{\text{M}}}{\text{EW}}\nabla\cdot\left(D_{\text{w}}^{\text{eff}}\nabla\lambda\right) + \nabla\cdot\left(n_{\text{d}}\frac{\sigma_{\text{p}}\nabla\phi_{\text{M}}}{F}\right) = 0 \tag{7}$$

Except for Eq. (3), the equations are common conservation equations in PEMFC literature. In treating Eq. (3), the cathode side of the cell is operated with SO_2-contaminated humidified reactants, normally in the order of several ppm in concentration in bulk. This situation yields a multicomponent transport of 4 species *i* consisting of O_2, N_2, SO_2 and water vapor. There will be interactions in between each species in the flow domain, which requires a simultaneous treatment of their respective fluxes. In this work, the Linearized Theory [12, 13] is used in order to simultaneously solve the mole fraction of each species in steady state.

3.2. Source Terms

Table 1 lists the forms of source terms *S* used in Eqs. (1 – 7) in the gas channel, GDL and membrane.

Table 1: Source terms

	Gas channel	GDL	Membrane
Smom	0	$-\varepsilon u \frac{m}{K_p}$	–
Sspe,i	0	0	–
Sch,s	0	0	–
Sch,M	–	–	0
Sene	0	$s_s^{\text{eff}} \|\| f_s \|\|^2$	$s_p^{\text{eff}} \|\| f_M \|\|^2$
Sliq	–	$\varepsilon \dot{m}_{\text{l-v}}$	–
Sspe,H2O	0	$-\varepsilon \dot{m}_{\text{l-v}}$	–

In Table 1, $\dot{m}_{\text{l-v}}$ [kg/(m^3.s)] can be calculated via condensation and evaporation process from [11].

4. Modeling SO_2 Contamination Kinetics

4.1. Oxygen Reduction Reaction (ORR) at Cathode Catalyst Layer under SO_2 Contamination

The catalyst layer is made of Pt nanoparticles supported on carbon mixed with membrane ionomer. ORR occur at the so-called 'active sites' which are the three-phase boundary of Pt, carbon and ionomer [11]. There are two most probable and debated mechanisms for ORR namely the associative and dissociative mechanisms. Both mechanisms can be considered, albeit the 4-electron transfer associative mechanism seems to be preferable for a wider range of potentials [14]. In this work, the ORR at cathode is assumed to follow the dissociative mechanism [14] below due to the availability of its kinetics data in [15]. In a SO_2-contaminated cathode electrode, the ORR mechanism during its sequential execution will be preceded by a competitive adsorption of O_2 and SO_2. This can written as

Competitive adsorption:

$$O_2 + 2Pt \underset{k_{1b}}{\overset{k_{1f}}{\rightleftarrows}} 2Pt\text{-}O \quad \text{(R1)}$$

$$SO_2 + 2Pt \underset{k_{2b}}{\overset{k_{2f}}{\rightleftarrows}} Pt\text{-}SO_2 \quad \text{(R2)}$$

Charge transfer reactions:

$$Pt\text{-}O + H^+ + e^- \underset{k_{3b}}{\overset{k_{3f}}{\rightleftarrows}} Pt\text{-}OH \quad \text{(R3)}$$

$$Pt\text{-}OH + H^+ + e^- \underset{k_{4b}}{\overset{k_{4f}}{\rightleftarrows}} Pt\text{-}H_2O \quad \text{(R4)}$$

$$Pt\text{-}H_2O \underset{k_{5b}}{\overset{k_{5f}}{\rightleftarrows}} Pt + H_2O \quad \text{(R5)}$$

Obviously in this case, the surface coverage on Pt is

$$q_O + q_{SO_2} + q_{OH} + q_{H_2O} + q_{Pt} = 1 \quad (8)$$

while the surface coverage on ionomer is

$$q_{H^+} + q_{\text{ionomer}} = 1 \quad (9)$$

R1, R2, R4 and R5 are reactions in equilibrium, which has fast kinetics. By defining $f = F/R_uT$, the surface coverage of adsorbates on cathode electrocatalyst layer can be written as a function of surface partial pressure of gases P_i as

$$\theta_O = \frac{1}{B_c}\sqrt{K_1 P_{O_2}}, \quad \theta_{SO_2} = \frac{1}{B_c}\sqrt{K_2 P_{SO_2}}, \quad \theta_{OH} = \frac{1}{B_c}\left[\frac{P_{H_2O}}{K_5} e^{f(E_c - E_c^\Phi)}\right]$$

$$\theta_{H_2O} = \frac{1}{B_c}\left(\frac{P_{H_2O}}{K_5}\right), \quad \theta_{Pt} = \frac{1}{B_c}$$

$$B_c = \sqrt{K_1 P_{O_2}} + \sqrt{K_2 P_{SO_2}} + \frac{P_{H_2O}}{K_5} e^{f(E_c - E_c^\Phi)} + 1 \quad (10)$$

One of the elementary step reactions R1 – R5 must be the rate-determining step (RDS). In this work, R3 is assumed to be the RDS, and its net current density depends on the cathode potential that can be written as

$$i_c = Fk_3^0\left[\theta_O \theta_{H^+} e^{-\alpha f\left(E_c^{Eq} - E_c^\Phi\right)} - \theta_{OH} e^{(1-\alpha) f\left(E_c^{Eq} - E_c^\Phi\right)}\right] \quad (11)$$

At E_c^{Eq}, the exchange current density $i_{0,c}$ can be derived by identifying k_3^0 to be the cathode RDS apparent standard rate constant k_c^0 in the ORR mechanism as

$$i_{0,c} = Fk_c^0 \theta_O^* e^{-\alpha f\left(E_c^{Eq} - E_c^\Phi\right)} = Fk_c^0 \theta_{OH}^* e^{(1-\alpha) f\left(E_c^{Eq} - E_c^\Phi\right)} \quad (12)$$

This leads to an equation of the cathode local current density i_c as a function of local cathode overpotential η_c

$$i_c = i_{0,c}\left[\frac{q_O}{q_O^*} e^{-a f \eta_c} - \frac{q_{OH}}{q_{OH}^*} e^{(1-a) f \eta_c}\right] \quad (13)$$

in which the value of $i_{0,c}$ is calculated using Eq. (10) below,

$$i_{0,c} = Fk_c^0 \left(q_O^*\right)^{1-a} \left(q_{OH}^*\right)^a \quad (14)$$

4.2. Closed-form Activation Overpotential Expressions

Equation (13) can be rearranged to solve for the activation overpotential as a function of current density and the coverage of the adsorbates. A general form applicable to both electrodes is obtained:

$$\eta = \frac{R_u T}{F}(x - g) \quad (15)$$

The procedures to obtain calculation parameters ξ and γ is detailed elsewhere [11].

4.3. Thermodynamically-Optimized Kinetics

The equilibrium constants *K* in Eq. (10) is found from $K = k_{nf}/k_{nb}$. The rate constants $k_{nf/b}$ must be found from thermodynamically optimized adsorption-desorption kinetic data. A more recent data from [15] is adopted for ORR, and from [16] and [17] for SO_2, which can be viewed in Table 2.

Table 2: Adsorption-desorption kinetic parameters for rate constant calculations from Hauptmann et al. [15], Benzinger et al. [16] and Sharma et al. [17].

Rn[a]	$s_{0,n}$ [-] or A_n [s^{-1}][b]	β_n [-]	$\tilde{E}_{a,n}$ [kJ/mol]
R1f	0.0542	0.77	-
R1b	8.41×10^{12}	0.93	$211 - 134\theta_O$
R2f	0.5	0.0	-
R2b	1.00×10^{16}	0.0	91.8
R5f	0.108	1.16	-
R5b	2.03×10^{12}	2.49	$40 - 10\theta_{H2O}$

[a] *f: forward (adsorption), b: backward (desorption)*
[b] *Values below 1.0 indicate sticking coefficients, otherwise are pre-exponentials*

The forward and backward rate constants k_{nf} and k_{nb} for the catalytic reactions are computed using a modified Arrhenius expression [11].

5. Numerical Solution Methodology

The modeling results from this study will be compared with published literature data from Mohtadi et al. [1]. The input operating parameters of the model cell, and the material properties are made to follow strictly the parameters as reported. The PEMFC used for comparison is a single cell with a triple path serpentine flow field with a PRIMEA Series 5621 MEA (Gore) sandwiched to Carbel CL GDL (Gore). Humidified high-purity oxygen gas with two values of bulk SO_2 concentrations (in ppm) is supplied at cathode. The cell is operated in a co-flow arrangement. The stoichiometric value is fixed to 2.0 to cathode at each current density to which their respective flow rates are calculated.

5.1. List of Assumptions

The list of assumptions made in this work includes:

- Only cathode electrodes are contaminated with SO_2. In actual operation SO_2 would probably being drawn inside the PEMFC through contaminated air at cathode, study in [8] revealed SO_2 crossover towards the anode through the membrane could occur.
- The differences that arise by using parallel triple path serpentine flow field in the experiment compared to the straight parallel flow field in this study are negligible. In actual operations the former has an advantage of better fuel utilization, but due to the pre-set stoichiometry value, it is assumed that fuel utilization is unaffected regardless of the channel flow geometry.
- The gas mixture obeys ideal gas law and its flow is steady, laminar and incompressible.
- The catalyst layers are treated as a two-dimensional planar interface in between GDL and membrane consisting of void, ionomer and solid Pt supported on carbon.
- The gas diffusion layer (GDL) is made from a material that is isotropic and homogeneous.
- Electrical contact resistance at the all interfaces is negligible.
- The solid and fluid phases are in thermal equilibrium over the GDL porous structure

5.2. Boundary Conditions

The boundaries for the calculation domain are marked with Roman numerals in Fig. 2. In short, no-flux boundary conditions are applied to symmetry boundary **II** and outlet boundary **IV** for the three-component velocity vectors and scalar variables. At the inlet boundary **III**, the inlet velocity u_{in} is prescibed. The O_2 inlet mole fraction is calculated using

$$X_{O_2,in} = 0.21\left(1 - j_c \frac{P_{sat@T}}{P_c} - X_{SO_2,in}\right) \tag{16}$$

The inlet temperature at this boundary is a constant made equivalent to the cell temperature. Boundary **I** and **V** are solid walls to which no-slip condition is applied to the velocity vector components, and no-flux condition is applied for the species scalars. A fixed temperature and the iteratively computed half-cell potential is applied at boundary **I**.

Boundary **VI** is the cathode catalyst layer, which are treated in this model as a two-dimensional sophisticated planar interface between GDL and membrane that can provide relevant fluxes towards the computational nodes at adjacent locations. The surface reaction occurred here prescribes a local current flux. The conservation equations, when applied at the control volumes adjacent to where the catalyst layer is prescribed as boundary flux has a generic form of

$$\int_A \mathbf{n}\cdot(\rho\mathbf{u}\zeta)\,dA - \int_A \mathbf{n}\cdot(\Gamma\nabla\zeta)\,dA = S\Delta x\Delta z \tag{17}$$

where ζ is a generic variable and Γ is a generic diffusional conductance. The list applied source terms S relevant at the catalyst layer is tabulated in Table 3. Further details on how the boundary conditions are treated can be found in [11].

The conditions applied in the catalyst layers are mostly flux of the transport parameters under the effect of local rate of reaction (local current density) based on geometric surface area $\bar{i}_c$ [A/m^2]. Since rough electrode is used, the local current density based on geometric surface area is calculated as $\bar{i} = ir_f$, where r_f is the roughness factor. The roughness factor r_f is defined as $r_f = L_{Pt}A_{CL}$ [m^2_{Pt}/m^2].

Table 3: Source term S in the cathode catalyst layer as in Eq. (17).

S	Expression
S_{liq}	$\frac{\bar{i}_c}{2F}$
$S_{ch,s}$	$\bar{i}_c$
$S_{ch,M}$	$-\bar{i}_c$
S_{ene}	$\bar{i}_c\left(-\frac{T\Delta S_c}{2F} + \lvert h_c\rvert + \frac{\bar{i}_c y_{CL}}{(1-\varepsilon_{CL})s_s}\right)$

5.3. Closure Constitutive Relations

This work adopted a galvanostatic approach, which means that the model has the ability to compute the cathode overpotential by supplying to the model current density as input. By averaging the overpotentials over catalyst layer surface, the cathode potentials E_c is written as

$$E_c = E_c^{rev} - \frac{1}{A_{CL}}\int_{\Delta x}\int_{\Delta z}\lvert h_c\rvert\,dz\,dx \tag{18}$$

where $E_c^{rev} = 0.0025T + 0.2329$ [18]. The final cell potential as used in the polarization curve then is calculated as

$$E_{cell} = E_c - \bar{i}R_{ohmic}. \tag{19}$$

In this study, the membrane resistance R_{ohmic} is calculated as a function of its volume-averaged, hydration-dependent conductivity calculated by the relationship $R_{ohmic} = y_M/\sigma_p(\lambda)$. The electronic contact resistances at material interfaces are neglected in this study. The coupled partial differential equations (1 – 7) are discretized using finite volume method with power-law differencing, and solved via SIMPLE algorithm using an in-house developed solver written in FORTRAN. Convergence is determined when maximum error in the computational domain is less than 1.0×10^{-7}.

5.4. Parameters and Constants

The list of the parameters and constants used in this work can be found in Table 4. For the sake of brevity, unlisted parameters and the constitutive relations for the macro-homogeneous conservation equations are listed elsewhere [11].

6. Results and Discussions

The operating parameters and material properties used as input in this computational work follow closely the parameters reported in the experimental work of Mohtadi et al. [1]. This way, relevant model results can be compared with the experimental data, and the extent of the model's applicability and its potential for improvement can be made. Table 5 tabulated the operating conditions used in this work.

Table4: List of cell physical parameters and constants.

Parameter or constant	Unit	Value	Ref.
Channel width, z_c	m	3.00×10^{-3}	[-]
Channel length, x_c	m	2.00×10^{-2}	[-]
GDL thickness, y_{GDL}	m	4.60×10^{-4}	[1]
Membrane thickness, y_M	m	3.50×10^{-5}	[1]
Catalyst layer thickness, y_{CL}	m	5.00×10^{-5}	[19]
Porosity of GDL, ε	-	0.3	[20]
Permeability of GDL, K_p	m^2	1.3×10^{-11}	[21]
Molecular weight of sulfur dioxide, M_{SO2}	kg/mol	64.063	[22]
Electronic conductivity of GDL, σ_s	S/m	37.23	[23]
Catalyst loading, L_{Pt}	mg/cm^2	0.6	[1]
Geometric area, A_{CL}	cm^2	23	[1]
ORR RDS exchange current density, $i_{0,c}$	A/m^2_{Pt}	0.05	[-]

Table 5: Operating conditions as reported in [1]

Operating Condition/Item	Value/Description
Reactants	Air
Cell temperature, T	70°C
Cell pressure, P_c	1 atm (cathode)
Cell humidification, φ_c	100% RH (cathode)
Stoichiometry	2.0 (cathode)
Inlet SO_2 concentration	2.5, 5.0 ppm

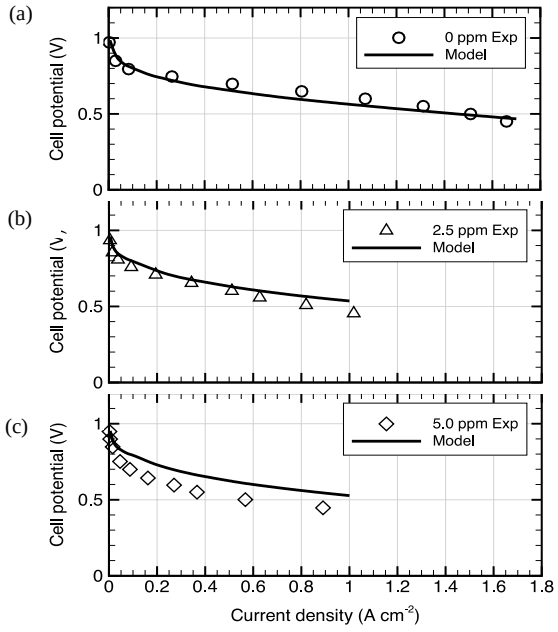

Fig. 3: Comparison between model prediction (line) and experimental [1] (symbols) current-potential (polarization) curve of a SO_2 contaminated PEMFC under variation of bulk SO_2 concentration in the air feed for (a) 0, (b) 2.5, and (c) 5 ppm SO_2. Only weakly adsorbed SO_2 is considered.

Figure 3 shows the comparison of the cell polarization obtained from model via Eq. (19) and the experimental data by Mohtadi et al. [1]. Comparison is done with respect to a variation in the bulk SO_2 concentration in the cathode air feed, namely 0, 2.5 and 5 ppm SO_2 is premixed in air and continuously supplied. Fig. 3(a) shows the cell polarization when operated without SO_2 contamination, and a general trend of decreasing cell potential with current density is seen. It is a common understanding that the source of this loss in cell potential is due to the intrinsic electrode overpotentials. Electrode overpotential is a cumulative effect of the losses in the cell, which can be from an intrinsically kinetic activation loss η_c, an ohmic loss and mass transfer-induced loss. The activation overpotential at the cathode electrode is known to be larger than its anode counterpart, due to its apparent rate constant is smaller by several orders of magnitude. This fact, combined with reactant transport resistance due to liquid water formation already made the cathode electrode sufficiently susceptible to be the main source of losses in the cell. Figure 3(a) is used to empirically determine ORR RDS apparent rate constants k_0, which are found to be 2.38×10^{-4} mol/(m^2_{Pt}s), respectively. This value is then applied to the subsequent cases with contamination, which is used to obtain Fig. 3(b) and 3(c).

Polarization curve in Fig. 3(b) shows the same cell but with a contaminated cathode electrode after being continuously supplied with 2.5 ppm SO_2 in the air feed. The effect of contamination is evident from both the experimental data and model prediction, in which the cell potential decreases with increasing electrode current density with a larger gradient compared to Fig. 3(a). The experimental data shows the loss in potential is ca. 0.15 V at 1.0 A/cm^2. The prediction model shows under-prediction of this value. Calculation using only weakly adsorbed SO_2-ad blocking the cathode active sites predicted the loss in potential to be only ca. 0.02 V at 1.0 A/cm^2, equivalent to an extent of 21% of error. This suggests that the major source of kinetic loss in the cathode electrode due to SO_2 contamination will be due to strongly adsorbed sulfur containing species. The interaction of sulfur dioxide on Pt or a carbon-supported Pt (Pt/C) whether in an electrochemical interface or otherwise still remains a highly complex phenomenon. The formation of the latter states of strongly adsorbed ad-species is suggested due to dissociation of the molecularly adsorbed SO_2 upon adsorption. Thermal decomposition of SO_2-ad into the SO-ad and S-ad is also possible for temperature above 300 K [24]. In an electrochemical interface, much earlier study in [4] suggests conversion to SO-ad and S-ad is from electrochemical reduction of SO_2-ad. Obviously, reduction of SO_2-ad in parallel with ORR pathway though evident will be a significant mathematical challenge.

Figure 3(c) shows the same cell now being continuously supplied with 5.0 ppm SO_2 in the air feed. A higher SO_2 concentration in the air feed will cause higher SO_2 mole fraction reaching/blocking the catalyst surface. This will aggravate the increase the cathode activation overpotential, and subsequently decrease the cell potential even more. The data shows an even larger gradient compared to Fig. 3(b), which confirms that the loss in potential will be much severe with increasing bulk SO_2 concentration. The experimental data shows the loss in potential is ca. 0.2 V at 0.9 A/cm^2. The prediction model on the other hand still shows under-prediction of this value. Similar to above, calculation using only weakly adsorbed SO_2-ad predicted the loss in potential at 0.9 A/cm^2 only ca. 0.03 V, equivalent to an even higher error of 25%.

Figure 4 shows the mole fraction distribution of O_2 and SO_2 respectively for the 2.5 ppm bulk SO_2 concentration case at 0.2 A/cm^2. The region above the dotted line is the gas channel, and below the dotted line is the porous GDL. Both figures are obtained by simultaneously solving the quaternary species conservation equation in Eq. (3), taking into account the effect of one species diffusive flux to the diffusive flux of other species inside a reacting flow setup. A reactant consumption flux at the catalyst layer (y = 0 mm) prescribes the amount of mole fraction the surface needed to solve for the surface coverage of the adsorbates.

Figure 4(a) indicates since air is used, the mole fraction of oxygen is already low, with the inlet O_2 partial pressure (or concentration) corresponding to 21% of the partial pressure of the incoming air supply. Higher surface mole fraction is predicted at the catalyst layer region directly under the channel compared to the ribs due to O_2 following the path of least transport resistance, which is, the shortest diffusion length. In Fig. 4(b) for SO_2, though the distribution is almost similar to O_2, the absence of reactant consumption leads to a relatively higher mole fraction under the channel. The mass of SO_2 transported here remains 'accumulated', which calls for a higher convection mass transfer should be applied in order to purge the excess mass.

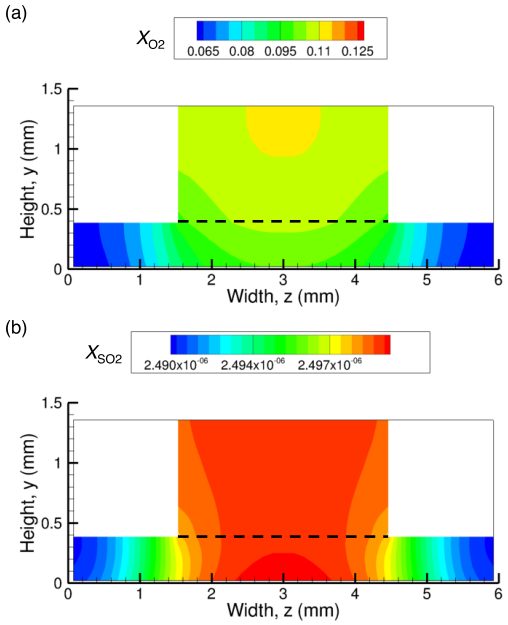

Fig. 4: Cathode side mole fraction distribution of (a) O_2 and (b) SO_2 at the location at channel exit (x = 20 mm) for the 2.5 ppm bulk SO_2 concentration case at 0.2 A/cm^2.

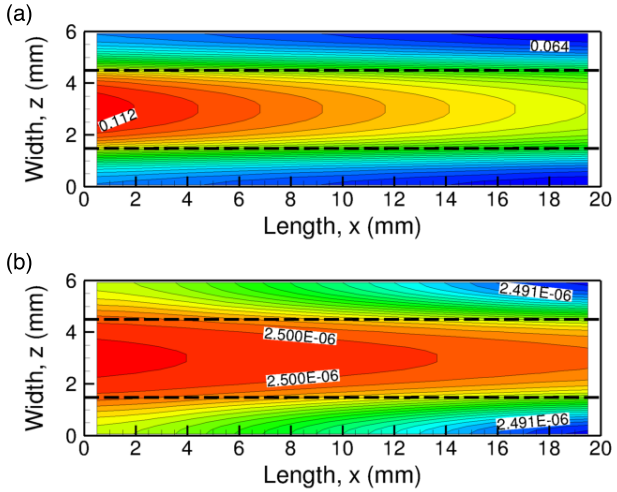

Fig. 5: Cathode side mole fraction distribution of (a) O_2 and (b) SO_2 at the catalyst layer for the 2.5 ppm bulk SO_2 concentration case at 0.2 A/cm^2. Region enclosed within the dashed lines is under the channel, otherwise ribs.

The along-channel contours of how the mole fraction of O_2 and SO_2 are distributed on the reacting catalyst layer are depicted in Fig. 5. In Fig. 5(a), the conversion of O_2 into surface ad-species, and later to H_2O via ORR leads to a decreasing profile along the channel. The distinct difference of higher mole fraction under the channel compared to under ribs is seen here as well. Judging from the spacing of the contours, the surface mole fraction gradient perpendicular to the flow (along z-axis) is consistently higher compared to the surface mole fraction gradient along the flow (x-axis). This shows the region under the channel is reactively more facile due to consistent availability of the reactants. In Fig. 5(b), absence of consumption leads to the surface mole fraction of SO_2 becomes rather uniform, with a very low mole fraction gradient under channel along flow. Lower value of SO_2 mole fraction is expected at hard-to-reach areas under the ribs near exit. However, in this reacting flow setup, information from mole fraction distribution alone might not paint an accurate picture of the kinetics of the electrode. In this study, a surface distribution of coverage of the participating adsorbates in a set reaction mechanism is emphasized to more representative of the kinetics, particularly when there is a competing reaction in place. Competing reactions on active surface sites are normally preceded by competitive adsorption of surface species. The following figure illustrates the results of the competition between O_2 and molecular SO_2 at the surface of cathode catalyst layer.

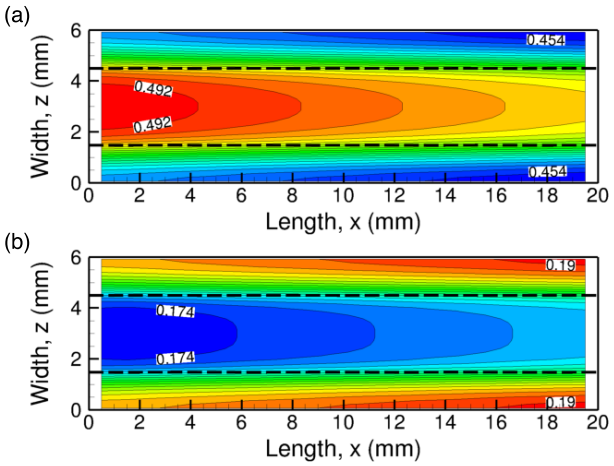

Fig. 6: Cathode side surface coverage distribution of (a) O-ad and (b) SO_2-ad at the catalyst layer for the 2.5 ppm bulk SO_2 concentration case at 0.2 A/cm^2.

Figure 6 shows the surface coverage distribution of dissociated atomic oxygen O-ad and molecular sulfur dioxide SO_2-ad at the GDL/membrane interface, which is treated in this modeling work as the catalyst layer. Both figures are for bulk SO_2 concentration of 2.5 ppm, and at nominal applied cell current density of 0.2 A/cm^2. The surface coverage distribution of O-ad in Fig. 6(a) shows a higher value under the channel compared to under the ribs, decreasing towards channel exit. Following dissociative ORR mechanism, coverage of O-ad on the catalyst layer at 0.2 A/cm^2 is predicted to be ca. 40 – 50%. The distribution of O-ad follows the distribution of O_2 mole fraction reaching the said interface via convection and diffusion, as depicted in Fig. 5(a). The surface coverage of weakly adsorbed molecular SO_2 is shown in Fig. 6(b). The computational model predicted coverage of weakly adsorbed SO_2 of less than ca. 20% on the catalyst surface at 0.2 A/cm^2, equivalent to less than 0.2 ML using the assumption of one adsorbate to adsorb on one Pt site. Contrary to the distribution of O-ad, SO_2-ad shows a slightly higher coverage under the ribs, and prescribed a minimum at the catalyst layer region near inlet. This is believed to be due to the intricate balance where a large coverage of O-ad will result into SO_2-ad coverage to fall since the maximum allowable coverage is unity.

7. Conclusions

A thermodynamically optimized model that bridges heterogeneous surface electrochemical reaction with macro-homogeneous two-phase and non-isothermal transport has been developed and solved in three-dimensions for a case of a PEMFC contaminated with

SO_2. Model results reveal a lower affinity of Pt to SO_2 at cathode. which results into lower SO_2-ad coverage. Higher O-ad coverage is found particularly at the region under the channel compared to under the ribs. The model results also confirm higher SO_2 bulk concentration increases the coverage of SO_2-ad. Comparison with experimental data confirms that the model is able to predict the trend of higher potential loss given higher bulk SO_2 concentration in the air feed. It is also concluded that inclusion of only weakly adsorbed SO_2 will under-predict the exact potential loss experienced by the cell. The major source of potential loss at cathode is believed to be the strongly adsorbed SO-ad and S-ad. These adsorbates need to be adopted into the model in order to better predict the severity of degradation of the cell due to SO_2 contamination.

Acknowledgement

The financial support from the Ministry of Higher Education, Malaysia, under the Fundamental Research Grant Scheme (FRGS), FRGS/1/2017/STG01/UNITEN/02/2, is gratefully acknowledged.

References

[1] R. Mohtadi, W-K. Lee, and J. W. Van Zee (2004), Assessing durability of cathodes exposed to common air impurities, *Journal of Power Sources*, vol. 138, pp. 216–225.

[2] O. A. Baturina and K. E. Swider-Lyons (2009), Effect of SO2 on the Performance of the Cathode of a PEM Fuel Cell at 0.5–0.7 V, *Journal of The Electrochemical Society*, vol. 156, no. 12, pp. B1423-B1430.

[3] Y. Nagahara, S. Sugawara, and K. Shinohara (2008), The impact of air contaminants on PEMFC performance and durability, *Journal of Power Sources*, vol. 182, pp. 422–428.

[4] A. Q. Contractor and H. Lal (1978), The Nature of Species Adsorbed on Platinum from SO_2 Solutions, *Journal of Electroanalytical Chemistry*, vol. 93, pp. 99-107.

[5] Y. Zhai, G. Bender, S. Dorn, and R. Rocheleau (2010), The Multiprocess Degradation of PEMFC Performance Due to Sulfur Dioxide Contamination and Its Recovery, *Journal of The Electrochemical Society* , vol. 157, no. 1, pp. B20-B26.

[6] K. Punyawudho, J. R. Monnier, and J. W. Van Zee (2011), SO_2 Adsorption on Carbon-Supported Pt Electrocatalysts, *Langmuir*, vol. 27, pp. 3138-3143.

[7] S. Tsushima, K. Kaneko, H. Morioka, and S. Hirai (2012), Influence of SO_2 Concentration and Relative Humidity on Electrode Poisoning in Polymer Electrolyte Membrane Fuel Cells, *Journal of Thermal Science and Technology*, vol. 7, no. 4, pp. 619-632.

[8] S. Tsushima, H. Morioka, K. Kaneko, and S. Hirai (2008), Effect of Relative Humidity on Contamination of Cathode and Anode Electrodes by Sulfur Dioxide in Air Stream in PEMFC, *ECS Transactions*, vol. 16, no. 2, pp. 1043-1050.

[9] J. St-Pierre (2010), Proton exchange membrane fuel cell contamination model: Competitive adsorption followed by a surface segregated electrochemical reaction leading to an irreversibly adsorbed product, *Journal of Power Sources*, vol. 195, pp. 6379–6388.

[10] Z. Shi et al. (2009), A general model for air-side proton exchange membrane fuel cell contamination, *Journal of Power Sources* , vol. 186, pp. 435–445.

[11] S. Hasmady, K. Fushinobu (2014), Inclusion of surface heterogeneity in bridging PEM fuel cell electrode contamination kinetics and transport via a competitive Langmuir-Freundlich isotherm, *Journal of Solid State Electrochemistry*, vol. 18 (12), pp. 3387 – 3405.

[12] H. L. Toor (1964), Solution of the Linearized Equations of Multicomponent Mass Transfer, *AIChE Journal*, vol. 10, no. 4, pp. 448-465.

[13] R. Taylor and R. Krishna (1993), *Multicomponent Mass Transfer*. New York: John Wiley & Sons.

[14] V. P. Zhdanov and B. Kasemo (2006), Kinetics of electrochemical O2 reduction on Pt, *Electrochemistry Communications*, vol. 8, pp. 1132-1136.

[15] W. Hauptmann, M. Votsmeier, H. Vogel, and D. G. Vlachos (2011), Modeling the simultaneous oxidation of CO and H_2 on Pt – Promoting effect of H_2 on the CO-light-off, *Applied Catalysis A: General* , vol. 397, pp. 174-182.

[16] W. Benzinger, A. Wenka, and R. Dittmeyer (2011), Kinetic modelling of the SO2-oxidation with Pt in a microstructured reactor, *Applied Catalysis A: General* , vol. 397, pp. 209-217.

[17] H. N. Sharma et al. (2014), SOx Oxidation Kinetics on Pt(111) and Pd(111): First-Principles Computations Meet Microkinetic Modeling, *Journal of Physical Chemistry C*, vol. 118, pp. 6934-6940.

[18] V. Gurau, H. Liu, and S. Kakac (1998), Two-Dimensional Model for Proton Exchange Membrane Fuel Cells, *AIChE Journal*, vol. 44, no. 11, pp. 2410-2422.

[19] S. Hasmady, K. Fushinobu, and K. Okazaki (2009), Treatment of Heterogeneous Electrocatalysis in Modeling Transport-Reaction Phenomena in PEFCs , *Thermal Science & Engineering* , vol. 17, no. 4, pp. 147-156.

[20] K. T. Jeng, S. F. Lee, G. F. Tsai, and C. H. Wang (2004), Oxygen mass transfer in PEM fuel cell gas diffusion layers, *Journal of Power Sources* , vol. 138, pp. 41-50.

[21] J. Ihonen, M. Mikkola, and G. Lindbergh (2004), Flooding of Gas Diffusion Backing in PEFCs: Physical and Electrochemical Characterization, *Journal of The Electrochemical Society*, vol. 151, no. 8, pp. A1152-A1161.

[22] Y. A. Cengel and M. A. Boles (1998), *Thermodynamics: An Engineering Approach*. New York: McGraw-Hill.

[23] E. Yli-Rantala et al. (2012), Advanced Material Solutions for PEM Fuel Cells (Phase 2) – Final Report, VTT Technical Research Centre of Finland.

[24] Y-M. Sun et al. (1994), SO_2 adsorption on Pt(111): HREELS, XPS and UPS study, *Surface Science*, vol. 319, pp. 34-44.